16th World Conference on Earthquake, 16WCEE 2017

Santiago Chile, January 9th to 13th 2017

Paper N° 2641

Registration Code: S-V1464646459

FLEXURAL BEHAVIOR OF SCREEN-GRID INSULATED CONCRETE FORMS UNDER IN-PLANE LOADING

A. Lopez [1] and G. Leiva [2]

[1] *M.Sc, Universidad Federico Santa María, alvlopez@pdx.edu*
[2] *Professor, Universidad Federico Santa María, gilberto.leiva@usm.cl*

Abstract

This paper presents the obtained experimental and analytical results that permitted to describe the flexural behavior of the screen-grid ICF panels, as well as to define the parameters needed to carry out a Performance-Based Seismic Design procedure. Eleven test specimens were constructed and tested under monotonic and cyclic in-plane lateral loading. Test units were divided into two groups, each one constructed using different prefabricated forms made of expanded polystyrene. The first group included seven walls 120 cm long, 213.5 cm high and 20 cm thick. The rest of the specimens had the same nominal thickness and height, but they had a T-shaped cross section of 116 cm length. All the specimens were designed and detailed to obtain a response controlled by flexural behavior. Results showed a ductile and stable response controlled by flexure for all the test specimens, with yielding of the longitudinal reinforcement and compression failure of the concrete extreme fibers. This study permitted to conclude that screen-grid ICF walls can reach important deformations in the nonlinear range, as well as, a stable response, similar to that of conventional RC walls with similar geometric properties. Furthermore, it was verified that the flexural resistance model for solid RC members is applicable for these elements, taking into account section discontinuities. It was also verified that common cyclic non-linear flexural behavior models are applicable for this type of walls. As a result, performance levels for these elements were defined in terms of the expected lateral displacements. Finally, a typical low-rise residential building in Chile was analyzed and designed based on the results of this study.

Keywords: Insulated Concrete Form; Flexural behavior; In-plane loading; Performance-Based Seismic Design.

1. Introduction

Current seismic design provisions seek to provide to structures not only resistance, but also an adequate deformation capacity in the nonlinear range to satisfy the demand imposed by severe earthquakes. To meet this objective, it is advisable to design the structures to obtain a ductile flexural mode of failure, avoiding brittle modes like shear. Therefore, in order to develop adequate design models, it will be necessary to provide enough information to understand the actual behavior of structural elements. The aforementioned conditions are the key part in the process of developing new structural systems. Among these new systems, Screen-grid Insulated Concrete Forms (ICF) walls have become popular in residential construction, due to thermal and acoustic insulation properties, as well as its constructive characteristics. Screen-grid ICF walls are made of cast-in-place concrete using lightweight hollow precast forms. Generally, high-density expanded polystyrene foam is utilized for these forms because it allows to place both longitudinal and transverse reinforcement in its internal cores.

Due to the lack of experimental validated information about its seismic performance, ICF construction has not been approved to be used in low-rise building, especially in regions of high seismic risk. Furthermore, seismic performance factor for ICF wall constructions has not been studied nor included in current seismic provisions. In Chile, particularly, screen-grid ICF walls have been used only in residential housing up to two stories. Consequently, it becomes necessary to generate information that permits to characterize the seismic behavior of ICF walls, in particular, to expand the experimental database. Monotonic test results have shown that in-plane lateral resistance and stiffness of ICF walls is higher when compared with wood and steel stud walls of the same height/length aspect ratio [1]. In-plane cyclic test results have shown that, independent of the height/length aspect ratio and the axial load, for walls with same features, the global behavior of the wall is defined by the behavior of the vertical elements, and that axial load increases the lateral resistance and delays the stiffness degradation, especially in walls with higher height/length aspect ratio [2]. The objective of the research described in this paper was to validate a flexural strength model to characterize the seismic behavior of ICF wall. To fulfil this objective, a series of eleven screen-grid ICF walls were built and tested at the laboratory. Analysis of the experimental results permitted to verify the seismic design of a typical low-rise residential building in Chile, and to quantify the seismic performance factors of the system.

2. Flexural Strength Model

Theoretical flexural strength assessment of screen-grid ICF walls is based on cross-section analysis, as shown in Fig. 1. As a reinforced concrete construction, it has been assumed that the hypothesis of flexural theory is valid, which means that initially plane sections remain plane after bending, and reinforcement does not slip relative to concrete. The model considers the gaps created by the forms between concrete cores in the compression zone to obtain the resultant compressive force.

Analysis of the moment-curvature response allows to characterize the cross-section behavior from deformation compatibility and equilibrium conditions, and stress-strain relations for concrete and reinforcing steel. The nominal strength (M_n) of the member cross section is calculated imposing a maximum compressive strain of 0.003 in./in. at the extreme compressive fiber of the concrete. Mander model [3] for unconfined concrete and typical steel stress-strain model with hardening for reinforcing steel are considered in the moment-curvature analysis.

Lateral displacement at the top of the wall due to flexure is obtained using the curvature distribution along the height as shown in Fig. 1, in a similar way of conventional RC walls. Before yielding, a linear distribution of the curvature is integrated over the height. After yielding, a plastic hinge is formed at the base of the wall that provides non-linear deformation to the wall. If ϕ is the curvature after yielding, ϕ_y is the yield curvature, L_p is the plastic hinge length, H is the height of the wall, the theoretical flexural displacement after yielding is given by Eq. (1):

$$\Delta = \left(\frac{\phi_y \cdot H^2}{3}\right) + \left(\phi - \phi_y\right) \cdot L_p \cdot \left(\frac{H - L_p}{2}\right) \tag{1}$$

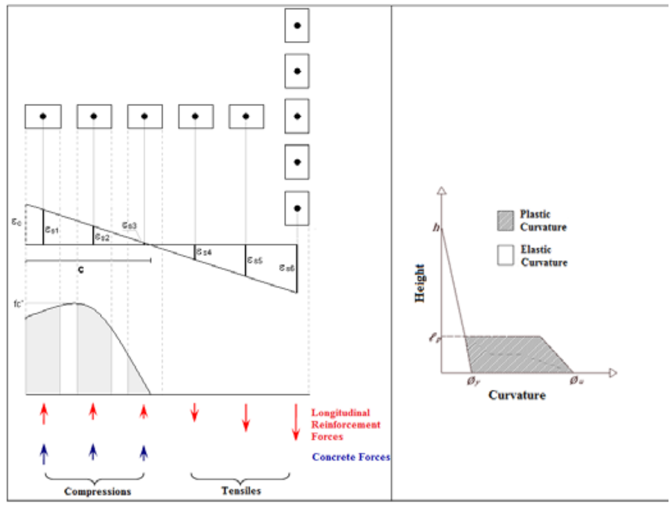

Fig. 1 – Conceptual flexural strength model and curvature distribution over the height

3. Experimental Study

3.1 Specimen details

In this study, eleven screen-grid ICF walls were designed, constructed, and tested at the laboratory. Specimens were divided into two groups, each one built using a different type of form. Being of a similar material, size and spacing of the reinforced concrete cores varied depending on the form manufacturer. ICF forms had openings that when stacked on top of another formed a grid of rectangular openings running both horizontally and vertically. Test specimens of the first group were of rectangular cross section, with nominal dimensions of 120 cm long, 20 cm thick, and they have a height of 213.5 cm. The walls were made of forms that measured 120 x 30.5 x 20 cm, and their openings were 13.2 x 10 cm, and spaced 20 cm center-to-center horizontally and 30.5 cm center-to-center vertically. The second group consisted of four T-section walls, with nominal dimensions of 116 cm long, 18.75 cm thick, and the same height of the first group. The forms used for this group measured 103.1 x 31.5 x 18.75 cm, and their openings were 11.75 x 11.75 cm, and spaced 18.75 cm center-to-center horizontally and 30 cm center-to-center vertically. Specimens were tested as simple vertical cantilevers. Each wall was rigidly secured to the laboratory strong-floor through a reinforced concrete foundations block. A rectangular (25 x 25 cm) RC beam was constructed at the top to transmit the lateral load to the specimen.

All the specimens were designed and detailed to obtain a response controlled by flexure. Longitudinal bars were placed at the center of the vertical concrete cores in all the units, except for specimens R6 and R7 where two hollow openings were joined at both ends creating boundary elements. All the longitudinal reinforcement was anchored 20 cm into the RC base with epoxy, and with 90^o hook to the top beam. Specimens were provided with ϕ8 tied transverse reinforcement, that was placed at the center of each horizontal concrete core and anchored with 180^o hooks around the extreme longitudinal bars, except for wall R3 were the ϕ8 was placed every two horizontal concrete cores. Additional ϕ8 stirrups were used in the boundary elements of specimens R6 and R7. Details of the longitudinal and transverse reinforcements, and values of the cylindrical concrete compressive strength (f'_c) measured at the time of specimens tests are presented in Table 1. Distribution of both longitudinal and transverse reinforcement on each specimen are depicted in Fig. 2.

3.2 Test Setup, Instrumentation and Loading Protocol

Each specimen was secured by the foundation beam to the laboratory strong floor using high-strength post-tension rods. Walls were tested under quasi-static reversed-cylic in-plane lateral load applied at their tops. No axial load was applied to the test units. The lateral load was applied by a hydraulic actuator attached to the RC loading beam, which reacted against the laboratory reaction wall. Specimens were permitted to move only in-plane. To prevent out-of-plane movement, steel braces were pin-connected at both ends of the RC loading beam and pinned at the laboratory floor. The instrumentation used for all the specimens consisted of linear variable differential transformers (LVDTs) positioned in such a way to monitor the in-plane wall deformation, rotations at wall bases, flexural and shearing deformations of wall sections, and potential slip and uplift relative to the laboratory floor. Load cells were used to measured applied in-plane lateral loads.

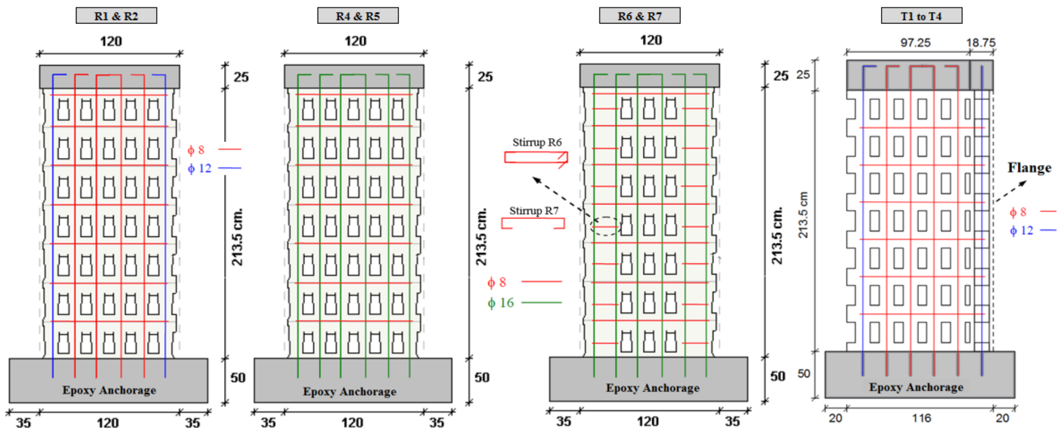

Fig. 2 – Specimen layouts

3.2 Test Setup, Instrumentation and Loading Protocol

Each specimen was secured by the foundation beam to the laboratory strong floor using high-strength post-tension rods. Walls were tested under quasi-static reversed-cylic in-plane lateral load applied at their tops. No axial load was applied to the test units. The lateral load was applied by a hydraulic actuator attached to the RC loading beam, which reacted against the laboratory reaction wall. Specimens were permitted to move only in-plane. To prevent out-of-plane movement, steel braces were pin-connected at both ends of the RC loading beam and pinned at the laboratory floor. The instrumentation used for all the specimens consisted of linear variable differential transformers (LVDTs) positioned in such a way to monitor the in-plane wall deformation, rotations at wall bases, flexural and shearing deformations of wall sections, and potential slip and uplift relative to the laboratory floor. Load cells were used to measured applied in-plane lateral loads.

Monotonic and cyclic tests were considered in this study. Specimens R2 and R4 (group I), and T1 and T4 (group II), were tested monotonically under displacement control at a rate of 3 mm/min. The rest of the specimens in both groups were subjected to the loading history shown in Fig. 3. Due to the high initial wall stiffness, cyclic tests were first conducted under load control until the theoretical yield capacity was reached. A displacement control procedure was used afterward. The loading history begins with three cycle series of increasing amplitude until flexural yielding is reached. After yielding occurs, the loading history continues with series containing cycles of degradation and cycles of stabilization. Degradation cycles aim to degrade the strength and stiffness of the element and consists of four cycles: 100%, 75%, 50%, and 25% of the maximum amplitude reached in the series. Stabilization cycles aim to stabilize the response and consists of three cycles of constant magnitude equal to the initial peak. The test protocol continues iterating the previous stages but increasing the initial peak of the series. The 20% reduction of strength criterion was used for assessing hysteretic behavior to limit excessive structural seismic drift.

3.3 Test Results

A summary of the test results is presented in Table 2. Observed mode of failure of each case, lateral force V, top displacement u, and drift ratio (displacement/wall height ratio) are presented for the maximum lateral load and end of the test. In the first group, since specimen R3 suffered a sudden blow of pressure at the start of the test, causing its cracking and surpassing the flexural yielding in one direction, test results for this wall are not included in this work. The rest of the walls tested cyclically exhibited a similar behavior in both directions, and therefore, top displacement and lateral force correspond to the average measured values. For the T-section walls, presented values correspond to those measured in the corresponding direction. Hereinafter, positive and negative sign are referred as tension and compression flange, respectively.

Table 1 – Specimen Details

Specimen	f'c Mpa	Edge Longitudinal Reinforcement	Web Longitudinal Reinforcement	Flange Longitudinal Reinforcement	Transverse Reinforcement (per form)	Edge Column Stirrup (per form)
R1	27.2	1ϕ12	4ϕ8	-	ϕ8	-
R2	26.0	1ϕ12	4ϕ8	-	ϕ8	-
R3	28.2	1ϕ12	4ϕ8	-	ϕ8 [(b)]	-
R4	27.7	1ϕ16	4ϕ16	-	ϕ8	-
R5	26.6	1ϕ16	4ϕ16	-	ϕ8	-
R6	25.1	2ϕ16	2ϕ16	-	ϕ8	ϕ8 hoop
R7	25.8	2ϕ16	2ϕ16	-	ϕ8	ϕ8 stirrup
T1	29.1	1ϕ12	4ϕ8	2ϕ8 + 1ϕ12[(a)]	ϕ10	-
T2	32.4	1ϕ12	4ϕ8	2ϕ8 + 1ϕ12[(a)]	ϕ10	-
T3	33.3	1ϕ12	4ϕ8	2ϕ8 + 1ϕ12[(a)]	ϕ10	-
T4	33.8	1ϕ12	4ϕ8	2ϕ8 + 1ϕ12[(a)]	ϕ10	-

[(a)] A 1ϕ12 was placed in the intersection between web and flange
[(b)] ϕ8 was placed every two blocks

3.1.1 Monotonic Tests

Specimens R2, T1, and T4 developed a flexural-dominated failure similar to conventional RC walls. Wall R2 showed a behavior characterized by a large amount of horizontal cracks in the tension side that spread out diagonally to the compression side, and crushing of concrete at the wall base, as shown in Fig. 4. The specimen reached a top displacement of 100.3 mm (4.4% drift ratio), and no loss in lateral strength was observed at ultimate stage. Specimen T1 was tested by tensioning the flange and without removing ICF material. Therefore, observation of crack initiation and crack pattern development were limited. Observation of failure mode was feasible after removing the ICF material. At a displacement of 42 mm (1.86% drift ratio), specimen suffered a sudden reduction in the lateral strength (about 48%) due to pull-out of the longitudinal bars on the tension side (flange), event that limited its deformation capacity. The wall reached a top displacement of 70.3 mm (3.11% drift ratio). Crushing of concrete at the wall base and buckling of the web edge reinforcement were observed at ultimate condition, as shown in Fig. 4. Wall T4, that was stripped away from ICF material prior testing, was tested by compressing the flange. Fracture of the edge longitudinal bar at the web occurred due to a sudden blow pressure, causing an 80% reduction of lateral strength capacity at a drift ratio of 1.90%. At ultimate condition, specimen reached a top displacement of 86.4 mm (3.82% drift ratio). It also exhibited a minimal damage in the compression flange, horizontal crack pattern on the tension side, and detachment between flange and web at base. On the other hand, specimen R4 showed primarily characteristics of shear-dominated failure due to its larger steel longitudinal ratio. Flexure cracks initiated diagonal cracking along the web and extended to the compression side. Compressive failure of the wall toe produced a sudden loss of lateral resistance. Although shear produced a significant damage, failure showed a flexural crack pattern on the tension side. Test unit reached a top displacement of 42.3 mm (1.87% drift ratio) at ultimate condition. The load-displacement history of these tests are shown in Fig. 4.

3.3.2 Cyclic Tests

Specimens of both groups failed by flexure reaching about 2% of drift ratio. In general, the specimens showed a ductile behavior with almost no strength degradation, as well as a high dissipating energy capacity and stable response. Specimens of the first group also showed an identical flexural response in both directions, but more damage was observed in one direction (Fig. 5). Nevertheless, walls R5, R6, and R7 exhibited a diagonal cracking pattern along the web in one direction. Broadly, specimens behaved similarly to solid RC walls, although some vertical elements presented double curvature until approximately flexural yielding, but did not affect final of the walls. It was also observed that strength and ductility were not improved by adding boundary elements and stirrups, as compared with the other walls. Specimens of the second group exhibited a well-defined flexural cracking progress that defined the ultimate condition of the test. As expected, more strength was observed when the flange was tensioned. In both groups, the ultimate condition was defined by crushing of concrete at the wall compression toes and out-of-plane instability.

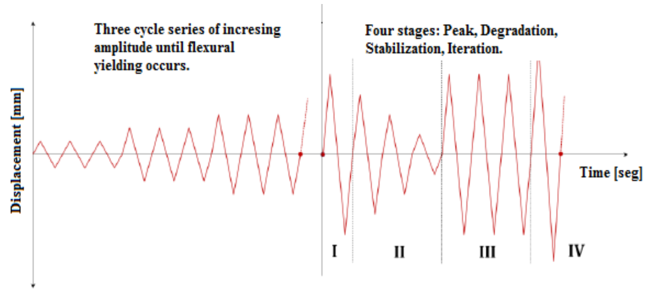

Fig. 3 – Loading History for cyclic tests

The load-displacement hysteresis curve and the damage pattern at ultimate state of specimen T3 are depicted in Fig. 6. Buckling of the edge longitudinal rebar was observed at a top displacement of 48 mm (2.12% drift ratio) when tensioning the flange. At the same time, crushing of the core concrete in compression web at wall toe occurred. In the second half of the same cycle (flange in compression), fracture of the edge reinforcing bar occurred, followed by a significant reduction in the lateral stiffness and strength of the wall (39.5 kN to 18.8 kN). Due to the severe damage at wall compression toe and loss of strength capacity, the test was ended at drift ratio of 2.47%. This wall presented a clear flexure-dominated failure governed by flexural crushing of concrete, buckling of flexural reinforcing and fracture of the edge reinforcing bar.

Table 2 – Test Results

Specimen	Loading History	Mode of Failure	Maximum Load			End of the Test		
			V_{max} [kN]	Δ_{Fmax} [mm]	Drift %	V_u [kN]	Δ_{max} [mm]	Drift %
R1	Cyclic	Flexure	47.2	30.2	1.34	44.3	44.3	1.96
R2	Monotonic	Flexure	50.4	65.0	2.88	43.1	100.3	4.44
R4	Monotonic	Flexure- Shear	95.5	33.2	1.47	64.2	38.4	1.70
R5	Cyclic	Flexure- Shear	91.1	30.0	1.33	84.1	40.7	1.80
R6	Cyclic	Flexure- Shear	91.5	30.5	1.35	89.2	37.8	1.67
R7	Cyclic	Flexure- Shear	92.1	17.0	0.75	88.8	39.2	1.73
T1	Monotonic	Flexure	114.7	36.6	1.62	50.0	70.3	3.11
T2 (+)	Cyclic	Flexure	115.7	24.0	1.06	93.4	39.9	1.77
T2 (-)		Flexure	53.9	24.0	1.06	29.7	39.9	1.77
T3 (+)	Cyclic	Flexure	120.6	24.0	1.06	86.6	55.7	2.46
T3 (-)		Flexure	56.9	24.0	1.06	18.8	48.0	2.12
T4 (-)	Monotonic	Flexure	64.7	33.0	1.46	16.1	86.4	3.82

4. Analysis of results

Analysis of the test results are summarized in Table 3. The yield displacement was obtained using an elastoplastic approximation of the cycle envelope. This approximation was achieved using the effective stiffness K_{eff}, which was computed as the secant stiffness at 75% of the peak lateral load. The horizontal part of the elastoplastic curve was assumed to pass through the peak lateral load V_{max}. The ultimate condition, represented by Δ_{20} and V_{20}, was defined as the maximum top displacement achieved or, when strength degradation occurred, as the displacement corresponding to a 20% drop in peak lateral load. The non-linear deformation demand is represented by the displacement ductility μ, calculated as the ratio of the displacements at ultimate condition to the displacement at flexural yielding. From the displacement ductility values, the curvature ductility μ_ϕ was computed according to Eq.2. Analysis of the results showed that using a plastic hinge length of 50% of the wall length provide accurate results.

$$\mu_\phi = \left(\frac{\phi_u}{\phi_y}\right) = \frac{H^2 \cdot (\mu - 1)}{3 \cdot L_p \cdot (H - 0.5 \cdot L_p)} + 1 \qquad (2)$$

4.1 Monotonic Tests

Specimen R2 showed the highest deformation capacity among the all the monotonically tested specimens. Comparing ductility values for specimens of the same shape, R2 showed higher values than R4. The difference is because R4 was designed with a longitudinal reinforcement ratio greater than the one used in R2. As for T-section walls, ductility values are relatively closed for both sense of loading, but being higher when the flange is in compression. In the case of specimen T4, ductility values might have been even higher if the blow of pressure had not occurred. After reaching its peak lateral load a few seconds after the start of the test, fracture of the edge longitudinal reinforcement in tension occurred and a strength degradation of about 80% occurred. In general, ICF units subjected to monotonic loading exhibited a good deformation capacity in the non-linear range of the response, with displacement ductility values ranging from 3.5 to 9.7.

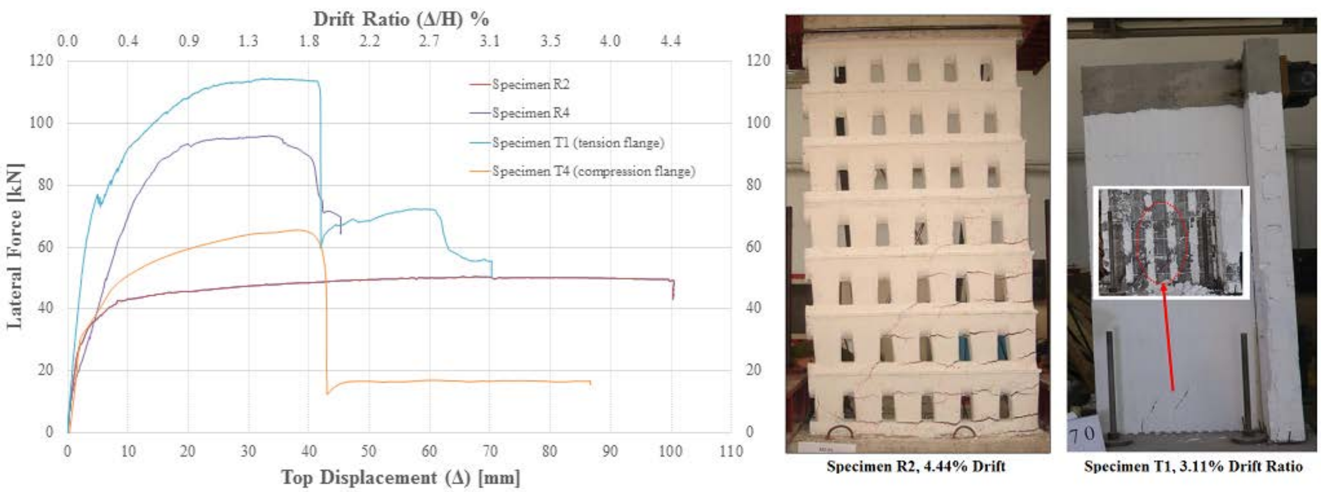

Fig. 4 – Load-Displacement history for monotonic tests and failure mode of walls R2 and T1

4.2 Cyclic Behavior

All test specimens developed flexural yielding during the tests. Additionally, all specimens were able to go further in the non-linear range of response, without undergoing a significant post-yield strength degradation. By comparing the hysteretic behavior of the two types of walls, rectangular ICF walls showed lesser strength degradation than T-section ICF walls.

Regarding the ductility values, a representative value was obtained for each type of section using cyclic tests. For T-section walls, an average of 4.2 when the flange is in tension and 4.9 when it is in compression. However, values for the flange in compression may be underestimated because of the rupture of the edge longitudinal rebar in tension. For rectangular section walls, an average value of 4.4 was obtained. As seen, this value is in between the ductility values for T-section walls. As for curvature ductility values, an average of 5.7 was obtained for rectangular walls, and 5.6 and 6.6 for T-section walls, tension and compression flange respectively.

The property of dissipating energy through hysteretic behavior is desirable in structures subjected to major seismic events. In this study the amount of energy that was dissipated by the specimens was calculated as the area enclosed by a full cycle for the first and last peak displacement cycle of each series of the hysteresis. Further, the energy dissipated in each cycle was normalized by the yield energy ($E_y = F_y \cdot \Delta_y$), which was computed from the corresponding monotonic test with similar features. Calculated energy ratios for specimen R1 and T3 are shown in Fig. 7. As seen, energy dissipation ratios rapidly degraded by the time wall deformation reached 0.5% drift, leveling to a relatively constant value thereafter.

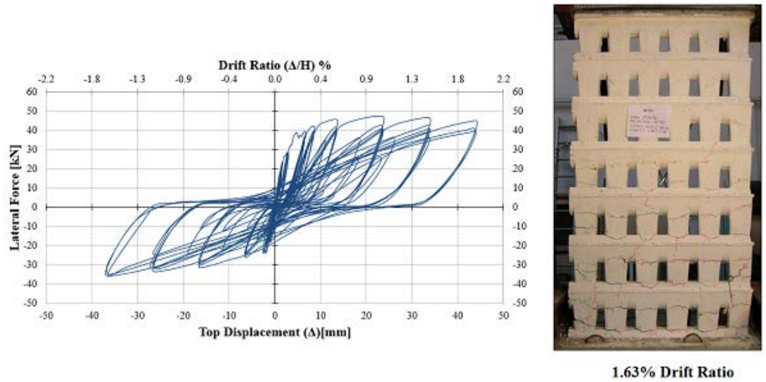

Fig. 5 – Cyclic response and ultimate condition of Specimen R1

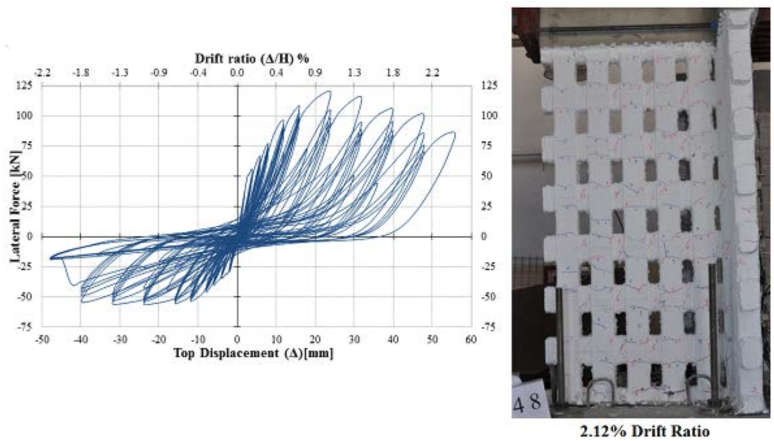

Fig. 6 – Cyclic response and ultimate condition of Specimen T3

5. Performance Based Design of Example Structure

A typical low-rise ICF residential housing was designed according to current Chilean seismic provisions. The obtained design was verified using the performance-based design approach. The procedure begins with a linear-elastic design, followed by a non-linear analysis of the structure. Non-linear models and parameters that characterized the hysteretic behavior of ICF walls are based on the obtained and calibrated experimental results presented in this work. The analysis aimed to obtain and/or verify theoretically the seismic performance factors of the ICF resisting system. Pushover and Time-History analysis were considered in the non-linear analysis procedure. The seismic performance factors were estimated in terms of the global inelastic response of the seismic-force-resisting-system obtained from the pushover curve, according to FEMA P695 procedure [4]. The system response modification factor R is defined as the ratio of base shear V_E the structure would developed during the elastic response for the design earthquake ground motion, to the design base shear V. The system overstrength factor Ω_0 is the ratio of the maximum lateral strength of the structure V_{max} to the design base shear V. The system deflection amplification factor C_d corresponds to the ratio of the roof displacement of the inelastic structure corresponding to the design spectra, δ, to the roof displacement corresponding to the design base shear, δ_E/R.

5.1 Description of the model

The analyzed building, depicted in Fig. 8, is a four-story structure with story-height of 2.44 m and RC slab of 12 cm thick. The structural system is composed only by ICF walls. Screen grid ICF walls are considered for the perimeter of the building. Due to fire resistance requirements, flat ICF walls are considered for the interior walls, which provide great stiffness to the structure. The building was analyzed and designed as per current seismic normative provisions [5]. The seismic load according to the relevant normative were estimated and the building was analyzed for combined effect of gravity and seismic loads. ETABS finite element software was utilized for the linear elastic three-dimensional modelling and analysis [6]. Furthermore, the model was analyzed for seismic zoning Z=3, importance factor I=1, soil class D. Since the ICF wall construction is a new seismic force-resisting system, no values are defined for the response modification factors in the current seismic normative [5]. However, the code allows to use ordinary shear walls in structural systems up to five floors, avowedly lesser ductile and that are designed using the factors R and R_0 less than or equal to 4. Hence, a response modification factor R_0=4 was used. Finally, all the walls were designed such that the behavior was flexural-dominated.

Table 3 – Analysis of Results

Specimen	K_{ef} kN/mm	Δ_y mm	Δ_{20} mm	Drift %	V_{20} kN	μ	μ_ϕ
R1	9.8	10.5	44.3	1.96	44.1	4.2	5.7
R2	6.9	10.4	100.3	4.44	44.1	9.7	13.7
R4	6.9	11.0	38.4	1.70	76.5	3.5	4.6
R5	6.9	9.8	40.7	1.80	87.3	4.2	5.6
R6	7.9	10.0	37.8	1.67	89.2	3.8	?
R7 (+)	7.9	9.3	39.2	1.73	90.7	4.2	?
T1 (+)	9.8	8.6	41.4	1.83	113.8	4.8	6.6
T2 (+)	7.9	11.2	39.9	1.77	93.2	3.6	4.7
T2 (-)	4.9	8.1	27.4	1.21	44.1	3.4	4.5
T3 (+)	8.8	10.7	50.8	2.25	96.1	4.7	6.5
T3 (+)	6.9	6.7	42	1.86	45.1	6.3	8.7
T4 (-)	5.9	8.2	41.6	1.84	60.8	5.1	7.0

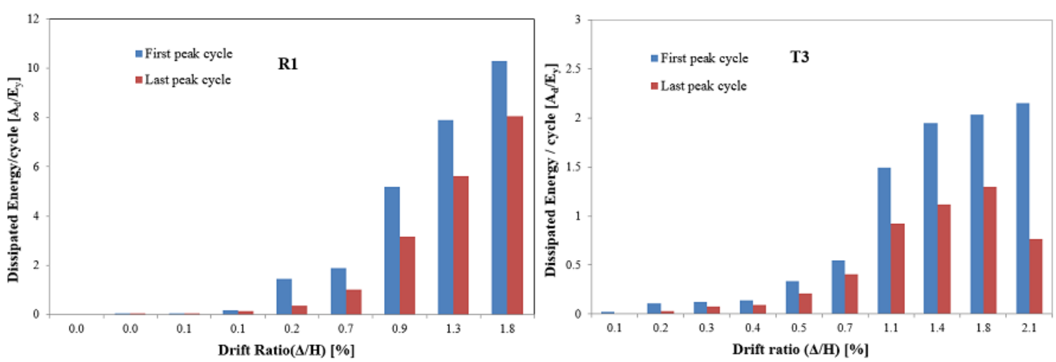

Fig. 7 – Energy dissipation ratio for first and last peak cycles

5.2 Non-Linear Analysis

Two-dimensional independent models were performed in both X and Y directions, using the software RUAUMOKO 2D [7]. The structure was modeled as fully fixed on its base and rigid diaphragm action on each floor to account for deformation compatibility. Non-linear models take into account the whole section of the walls, using their section properties according to the direction in study. Beam-column element properties must be entered as data, such as material properties as well as flexure and axial strengths. Experimental hysteresis curves of rectangular ICF walls that failed in flexure were calibrated by Matus [8] to characterize their nonlinear behavior. Modified Takeda hysteresis rule was calibrated for Pushover analysis [9]. Wayne-Stewart degrading stiffness with modified loop was calibrated for Time-History analysis [9]. Both hysteresis rules are shown in Fig. 9.

5.3 Pushover Analysis

Base shear versus roof drift curves were obtained for each direction. Curvature ductility μ_ϕ, obtained from the experimental results presented in this work, was used as representative parameter of the deformation capacity of the walls. For each type of wall, μ_ϕ was considered as the average of the curvature ductility values of the cyclic tests previously presented. As mentioned before, a curvature ductility of 5.7 was used for rectangular section walls, and 6.6 and 5.6 for T-section walls, compression and tension flange respectively. For those types of walls which no experimental information available, as C- and L-section walls, a representative value of μ_ϕ was used (i.e. for C-section walls in the X direction, μ_ϕ for T-section walls was used). For purposes of this study, the maximum roof displacement level is defined as the moment when the first wall reaches its ultimate deformation capacity. Therefore, the maximum acceptable roof drifts were 1.6% and 2.0%, X and Y direction respectively. Nevertheless, that criterion does not mean the collapse of the building. These values are coincident with the 1.5% roof drift proposed by Matus [8] as collapse prevention limit. Results for the system response modification and overstrength factors are presented in Table 4. As seen, the capacity of the structure is greater than the elastic demand prescribed by the current normative [5]. It can be seen, further, that the system showed a high overstrength level in both directions, explained by the presence of ICF flat walls in the central part, which provides a greater strength to structural system. These results showed that the structure should not undergone to inelastic response under a severe seismic event. System deflection amplification factor C_d values are summarized in Table 4. They were obtained using the capacity-demand-diagram method, defined in ATC-40 [10]. Fig. 10 shows the capacity-demand curves in both directions. The point where the capacity curve crosses the demand curve correspond to the performance point, that represents the maximum roof drift of the structure for the corresponding design spectra. As seen, the structure responded in the elastic range, but it must be verified with the Time-History results.

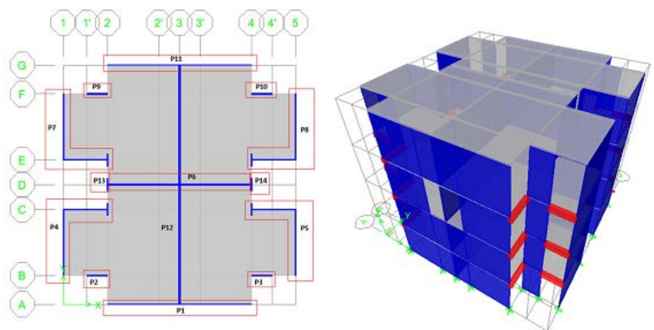

Fig. 8 – Low-rise ICF building model for numerical analysis

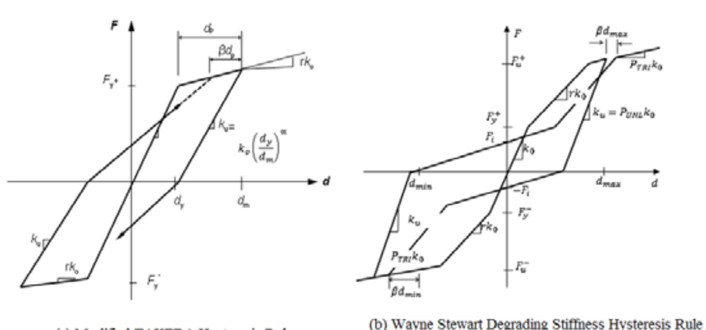

Fig. 9 – Hysteresis rules for nonlinear analysis

5.4 Time-History Analysis

Chile 1985 and 2010 ground motion records were used for the Time-history analysis in both X and Y directions. Fig. 11 depicts the global hysteresis curve of the building for Angol record. Even though this record was the most demanding for the structure, the inelastic response was minimum. By analyzing the moment-curvature curves of each wall, only the middle flat ICF wall in the X direction reached first flexural yielding at a drift ratio of 0.17%, but with no strength degradation in the hysteresis loops. The rest of the walls remained in the linear elastic range of response for all the records analyzed.

Table 4 – Seismic Performance Factors

Direction	V_E [kN]	V [kN]	R	V_{max} [kN]	Ω	δ_E/R [cm]	δ [cm]	C_d
X	2053.8	920.0	2.23	4776.0	5.2	0.14	2.0	14.3
Y	1981.2	920.0	2.15	5266.2	5.7	0.12	0.9	7.5

Comparisons between the peak drift ratio of each record with the performance point of the structure, showed that only Angol exceed those values, reaching a maximum of 0.35% and 0.15% drift ratio, X and Y direction respectively. Thus, it is verified that the resisting system in study will respond in the linear-elastic range of response. Moreover, these results validate the use of a response modification factor R_0=4 for buildings composed of ICF walls with similar features to the case of study, because no large ductility capacity is expected. Additionally, from the results obtained, low-rise buildings can be designed as ordinary RC shear walls, and therefore, it is not necessary to provide special boundary elements.

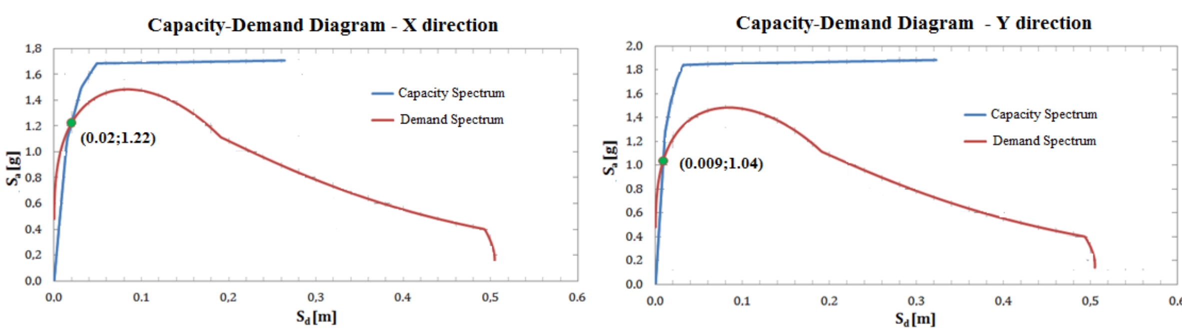

Fig. 10 – Capacity-Demand curves and performance point

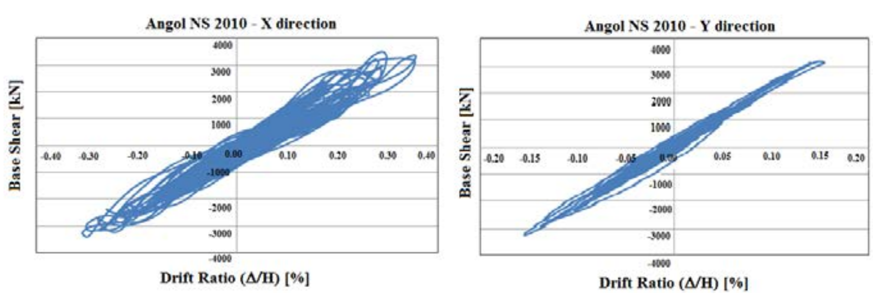

Fig. 11 – Time-History analysis for Angol NS

6. Conclusions

Test results have permitted to characterize the flexural behavior of screen grid ICF walls, and to verify the seismic performance of the analyzed building.

The analytical model presented in this paper is adequate to assess the nominal moment of screen-grid ICF walls of any cross section. Similarly, the deformation capacity in flexure is reasonably estimated using a plastic hinge length equal to 50% of the wall length. It is recognized that the behavior shown by the test units resemble a solid RC wall. Screen-grid ICF walls tested cyclically also exhibited a ductile behavior, with almost no strength degradation, as well as a high dissipating energy capacity and stable response. From the approximation used to compute the theoretical lateral displacement for ICF walls, representative values were obtained for the curvature ductility that allowed to establish values for the ultimate state of ICF walls that are in the performance level of collapse prevention.

Pushover analysis allowed to determine the deformation levels that the ICF building is able to develop, considering as a failure criterion the point at which the first wall reaches its deformation capacity based on the test results. The deformation levels were estimated in 1.6% and 2% drift ratio, X and Y direction respectively. Capacity-Demand spectrum method was used to obtain the performance point of the structure. Results shown that the structure responded in the linear-elastic range with maximum drift ratios of 0.2% and 0.1%, X- and Y-direction respectively. These results were verified by the Time-History analysis, in which the building responded in the linear range of deformation for the ground motion records considered in this study, with minimal or null nonlinear deformation. The results showed the building surpassed the performance point only for Angol-NS, with drift ratios of 0.35% (X-direction) and 0.15% (Y-direction).

Finally, it is concluded that a response modification factor R_o equal to 4 is advisable and provides good results, although more analysis need to be done to validate this value. System overstrength factor Ω_o is high due to the high flexural strength provided by the minimum reinforcement used in the design. As for the system deflection amplification factor C_d, it is high because of the small roof displacement corresponding to the design base shear, compared to the performance point.

4. Acknowledgements

This project, developed at the laboratory of the Federico Santa Maria Technological University, in Valparaiso, Chile, was sponsored by the Chilean Commission of Science and Technology, CONICYT, under grant Fondef D08I1165.

5. Copyrights

5. References

[1] Mehrabi, A. B. (2000). In-plane Lateral Load Resistance of Wall Panels in Residential Buildings. *Portland Cement Association*, R&D Serial No. 2043.

[2] Kay, T., Dusicka, P. (2011). In-plane Lateral Cyclic Behavior of Insulated Concrete Form Grid Walls. *Jorunal of Strcutural Engineering, ASCE*, Vol. 137.

[3] Mander, J.B., M.J.N. Priestley, R. Park. (1988). Theoretical Stress-Strain Model for Confined Concrete. *Journal of Structural Engineering*, Vol. 114, No. 8, pp. 1804-1826.

[4] Applied Technology Council. (2009). *Quantification of Building Seismic Performance Factors.* California: U.S., Federal Emergency Management Agency.

[5] Instituto Nacional de Normalizacion. (2012). *Norma chilena NCh 433 of.1996 Mod.2012, Diseño Sismico de Edificios.* Santiago.

[6] Computer and Structures, Inc. (2011). *ETABS, Extended 3D Analysis of Building System.* California: Computer and Structures, Inc.

[7] Carr, A. J. (1996). *Ruaumoko, Inelastic Dynamic Analysis.* Christchurch, New Zeland: Department of Civil Engineering, University of Canterbury.

[8] Matus, F. (2016). *Diseño Basado en Desempeño de Edificios de Muros ICF. Memoria para optar al titulo de Magister en Ciencias de la Ingenieria Civil.* Valparaiso, Chile: Universidad Tecnica Federico Santa Maria.

[9] Applied Technology Council. (1996). *Seismic Evaluation and Retrofit of Concrete Buildings.* California: Report ATC 40.